Paleoceanography and Paleoclimatology

RESEARCH ARTICLE
10.1029/2019PA003568

Dynamic Intermediate Waters Across the Late Glacial Revealed by Paired Radiocarbon and Clumped Isotope Temperature Records

Sophia K. V. Hines[1,2], John M. Eiler[1], John R. Southon[3], and Jess F. Adkins[1]

[1]Department of Geological and Planetary Sciences, California Institute of Technology, Pasadena, CA, USA, [2]Lamont-Doherty Earth Observatory, Columbia University, Palisades, NY, USA, [3]Earth System Science Department, University of California Irvine, Irvine, CA, USA

Key Points:
- Intermediate-depth waters are highly dynamic throughout the late glacial
- ϵ^{14}C and temperature crossplots from paired measurements show ocean endmembers across deglaciation
- Temperature and ϵ^{14}C data are outside the range of modern data in the N. Atlantic and Southern Ocean

Supporting Information:
- Supporting Information S1
- Tables S1–S7

Correspondence to:
S. K. V. Hines,
shines@ldeo.columbia.edu

Citation:
Hines, S. K. V., Eiler, J. M., Southon, J. R., & Adkins, J. F. (2019). Dynamic intermediate waters across the late glacial revealed by paired radiocarbon and clumped isotope temperature records. *Paleoceanography and Paleoclimatology*, *34*, 1074–1091. https://doi.org/10.1029/2019PA003568

Received 18 JAN 2019
Accepted 24 MAY 2019
Accepted article online 29 MAY 2019
Published online 10 JUL 2019

Abstract Paired radiocarbon and clumped isotope temperature records from U/Th-dated *Desmophyllum dianthus* corals in the North Atlantic and Southern Ocean provide unique information about the history of intermediate waters (~1,500–1,700 m) across the late glacial and deglaciation (~35–10 ka). These measurements allow for the construction of radiocarbon-temperature crossplots, which help to identify water mass endmembers at different times across the deglaciation. Radiocarbon and temperature values from the late glacial fall outside the range of modern ocean data from near the sample collection sites. In the North Atlantic, radiocarbon values tend to be much older than the modern, while in the Southern Ocean, they are more often younger than the modern. Reconstructed temperatures vary around respective modern ocean values; however, warm waters are observed at the Last Glacial Maximum and across the deglaciation in the north and south. We interpret our data in the context of the modern hydrography of the Western North Atlantic and Southern Ocean, and we draw upon direct comparisons between sediment core-derived reconstructions of ocean circulation from the South Indo-Pacific and our deep-sea coral data from the Southern Ocean. Our North Atlantic data support accepted patterns of reduced North Atlantic Deep Water formation during Heinrich Stadials 1 and 2. In the Southern Ocean, deep-sea coral populations respond to changes in ocean structure that are also reflected in a depth profile of δ^{13}C data from New Zealand, and data indicate that there was less influence of Pacific Deep Water between 1,500 and 1,700 m south of Tasmania across much of the deglaciation.

1. Introduction

Ocean circulation plays a central role in glacial-interglacial climate. Of particular importance is the meridional overturning circulation, which transfers water from the surface to the deep ocean on ~1,000-year timescales (Stuiver et al., 1983). The deep ocean is a crucial carbon reservoir in the ocean-atmosphere system, and small changes in circulation rate and structure can have a large impact on the pCO_2 of the atmosphere, which is closely linked to glacial cycles (Figure 1d; Barnola et al., 1987; Petit et al., 1999; Sigman & Boyle, 2000).

On shorter timescales during glacial periods, it has long been recognized that there is an antiphase relationship between high-latitude temperatures in the Northern and Southern Hemispheres, inferred from high-resolution ice core stable isotope records from Greenland and Antarctica (Figures 1b and 1c; Andersen et al., 2004; Bard, 2000; Barker et al., 2009; Blunier & Brook, 2001; Broecker, 1998; Crowley, 1992; Lamy et al., 2007; Rasmussen et al., 2014; WAIS Divide Project Members, 2013). These high-latitude temperature changes have been attributed to changes in the strength of North Atlantic Deep Water (NADW) formation (Figure 1e) and have been linked to atmospheric circulation and the strength of the Asian monsoon (Figure 1f). While surface ocean temperatures tend to follow ice core records, deeper ocean temperatures have not always followed surface temperature patterns. Clumped isotope and Mg/Ca records from the Nordic Seas show warmer temperatures in the high-latitude North Atlantic during the late glacial than the Holocene (Cronin et al., 2012; Thornalley et al., 2015), and deep-sea coral clumped isotope temperatures from the New England Seamounts show an abrupt warming event that precedes the beginning of the Bølling-Allerød warm period (14.7–12.8 ka) in the Northern Hemisphere (Thiagarajan et al., 2014). Modeling experiments across the deglaciation also show an accumulation of heat in the deep and intermediate Atlantic

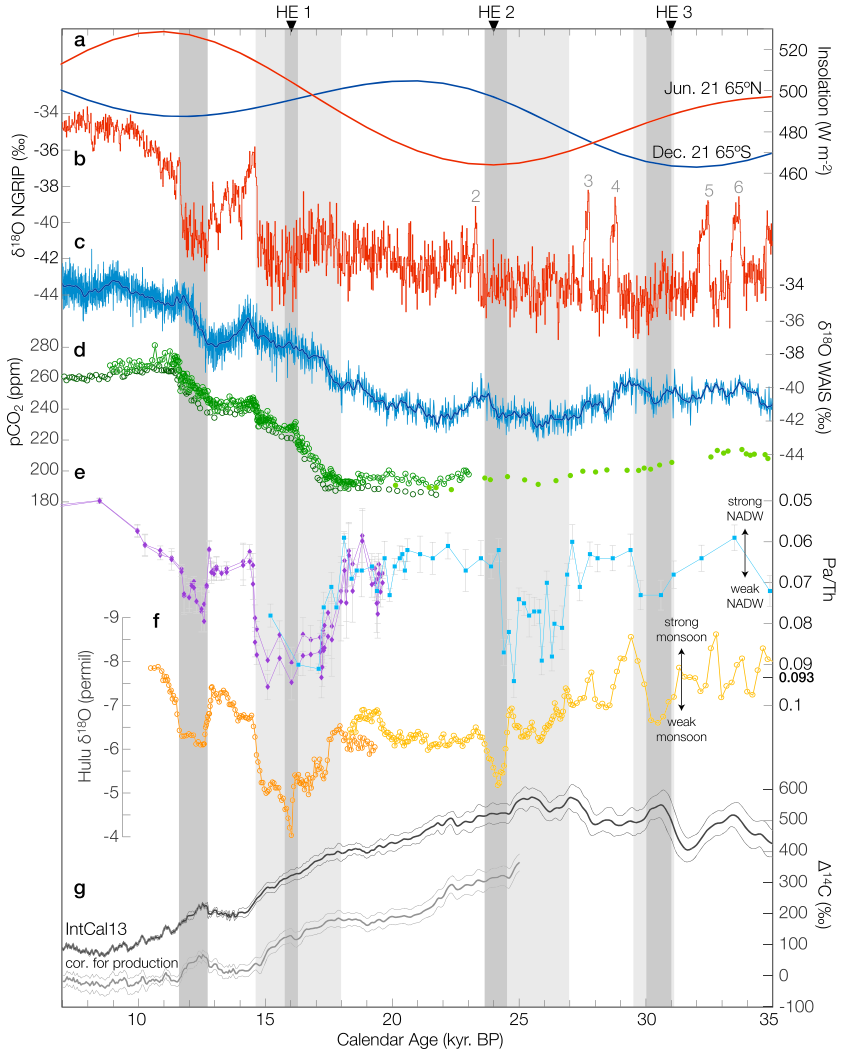

Figure 1. Compiled climate records spanning the late glacial. (a) High-latitude insolation curves (Huybers & Eisenman, 2006); (b) North Greenland Ice Core Project (NGRIP) $\delta^{18}O$ on the GICC05 chronology (Andersen et al., 2004; Rasmussen et al., 2014); (c) West Antarctic Ice Sheet (WAIS) $\delta^{18}O$ on the WD2014 chronology (Buizert et al., 2015; WAIS Divide Project Members, 2013); (d) atmospheric pCO_2 from WAIS (open circles and line; Marcott et al., 2014), EPICA Dome C (circles; Lemieux-Dudon et al., 2010; Monnin et al., 2001), and Taylor Dome (filled circles; Indermühle et al., 2000); (e) Pa/Th, a proxy for North Atlantic Deep Water (NADW) strength, from the Bermuda rise (purple diamonds; McManus et al., 2004) and ODP 1063 (blue squares; Lippold et al., 2009); (f) Hulu cave $\delta^{18}O$, a proxy for Asian Monsoon strength, from stalagmites PD (orange) and MSD (yellow; Wang et al., 2001); and (g) atmospheric $\Delta^{14}C$ from IntCal13 (Reimer et al., 2013) and the atmospheric $\Delta^{14}C$ record corrected for production (Hain et al., 2014). Light gray bars mark times of decreased NADW flux according to Pa/Th, dark gray bars mark weak monsoon intervals, and dates of Heinrich events are marked by triangles at the top of the figure (Hemming, 2004).

preceding the Bølling-Allerød, potentially driven by freshwater forcing in the North Atlantic (Dokken et al., 2013; Liu et al., 2009; Marcott et al., 2011).

In order to understand the asynchronicity between the hemispheres, and the ability of the ocean to store more carbon during glacial times, it is necessary to understand both the structure and rate of ocean circulation across the deglaciation. As was described by Talley (2013), in the modern ocean there is a "figure-eight"-like circulation: NADW that upwells in the Southern Ocean is far enough to the south that it experiences a negative surface buoyancy forcing and becomes part of sinking Antarctic Bottom Water (AABW). It is only once this AABW flows into the Indian or Pacific basins that it is able to diffusively upwell to a density class (Indian Deep Water or Pacific Deep Water [PDW]) where it can return to the Southern Ocean in a positive buoyancy forcing region, thus enabling the overturning circulation to close. There is

evidence that the structure of the ocean at the Last Glacial Maximum (LGM; ~22–18 ka) looked significantly different from the modern with a shoaled NADW, an expansion of AABW within the Atlantic basin and enhanced middepth stratification (Curry & Oppo, 2005; Lund et al., 2011). This shoaled NADW configuration would allow the overturning circulation to close within the upper cell because NADW would no longer upwell in a negative buoyancy forcing region in the Southern Ocean. We therefore think of this LGM circulation configuration as "two-cell" (Ferrari et al., 2014).

There is evidence not only that the structure of circulation during the LGM was distinct from the modern, but also that the stratification between northern and southern-source water was fundamentally different. Pore fluid measurements of ^{18}O and chlorinity, used as a direct measure of bottom water temperature and salinity, show that while the modern water column is dominantly temperature stratified, the glacial ocean was instead salinity stratified (Adkins, 2002). In order to better constrain circulation configuration at the LGM and the transitions into and out of the LGM state, it is useful to have more records with multiple geochemical tracers, especially physical tracers such as radiocarbon and temperature. Reconstructions with multiple physical tracers can give insight into the mechanisms driving observed signals, because different mechanisms correspond to different tracer-tracer relationships.

Radiocarbon is a well-established tracer of deep ocean circulation. Carbon-14 atoms are produced in the atmosphere, where they become incorporated into CO_2. Atmospheric $^{14}CO_2$ exchanges with surface ocean dissolved inorganic carbon, eventually coming to steady state, but when water leaves the surface, radiocarbon decays with a 5,730-year half-life. Therefore, the radiocarbon content of deep water is a measure of the amount of time that has elapsed since that water was at the surface (once the radiocarbon age of the surface water is taken into account). Since the deep ocean contains much more carbon than the atmosphere, the $\Delta^{14}C$ value of the atmosphere is also a sensitive indicator of changes in ocean circulation. Historically, radiocarbon has primarily been measured in planktic and benthic foraminifera; however, deep-sea corals also faithfully record the $\Delta^{14}C$ value of the water in which they grow (Adkins et al., 2002), and they have the added benefit of absolute age control via U/Th dating (Cheng et al., 2000; Lomitschka & Mangini, 1999).

Past deep ocean temperatures have been more difficult to constrain. Early measurements of oxygen isotopes on benthic foraminifera (Chappell & Shackleton, 1986; Emiliani, 1955; Shackleton, 1967) showed glacial-interglacial variation; however, $\delta^{18}O$ of carbonate is affected by both temperature and the $\delta^{18}O$ of the water (which varies with the growth and decay of ice sheets). Subsequently, Mg/Ca ratios in planktic (Nurnberg et al., 1996) and benthic (Elderfield et al., 2006; Martin et al., 2002; Rosenthal et al., 1997) foraminifera and surface corals (Mitsuguchi et al., 1996) were established as temperature proxies. Unfortunately, both of these methods for reconstructing paleo-deepwater temperature have proved complicated in deep-sea corals due to "vital effects," or ways in which the coral biology shifts isotope or elemental ratios away from theoretical values (Adkins et al., 2003; Chen et al., 2018; Gagnon et al., 2007).

Recently, a new paleothermometer has been developed for carbonates based on the thermodynamics of homogeneous isotope exchange in carbonate minerals. At cold temperatures, heavy carbon and oxygen isotopes tend to "clump" together within carbonate groups and at warm temperatures they tend to be more randomly distributed among carbonate groups within the mineral lattice (Eiler, 2007; Ghosh et al., 2006; Wang & Schauble, 2004). An initial study by Thiagarajan et al. (2011) indicated that there were no apparent vital effects for clumped isotopes in corals, but recently, this initial result has come into question (Spooner et al., 2016; Saenger et al., 2012). In shallow-water *Porites* corals, Saenger et al. (2012) found that offsets in clumped isotope value from the inorganic calibration line could be explained by incomplete equilibration of the CO_2 and DIC pools within the coral calcifying fluid as a result of rapid calcification. Deep-sea corals grow much slower than shallow-water corals, but a recent detailed study indicated that there are still small species-specific vital effects, with some species (*Balanophyllia*, *Dasmosmilia*, and *Enallopsammia*) affected much more strongly than others (*Caryophyllia*, *Javania*, and *Desmophyllum*; Spooner et al., 2016). While further inquiry into species-specific vital effects in deep-sea corals is warranted, our choice of *Desmophyllum dianthus* corals minimizes the possibility of bias.

In this paper, we present paired radiocarbon and temperature time series from North Atlantic and Southern Ocean intermediate waters derived from measurements of deep-sea corals from a narrowly restricted depth range (N.B. we use the term "intermediate water" to describe the depth of our samples even though they are not necessarily bathed in "Antarctic Intermediate Water" [AAIW]). In the modern Southern Ocean, temperature and radiocarbon distributions are broadly similar to each other and zonally symmetric (Figures 2a

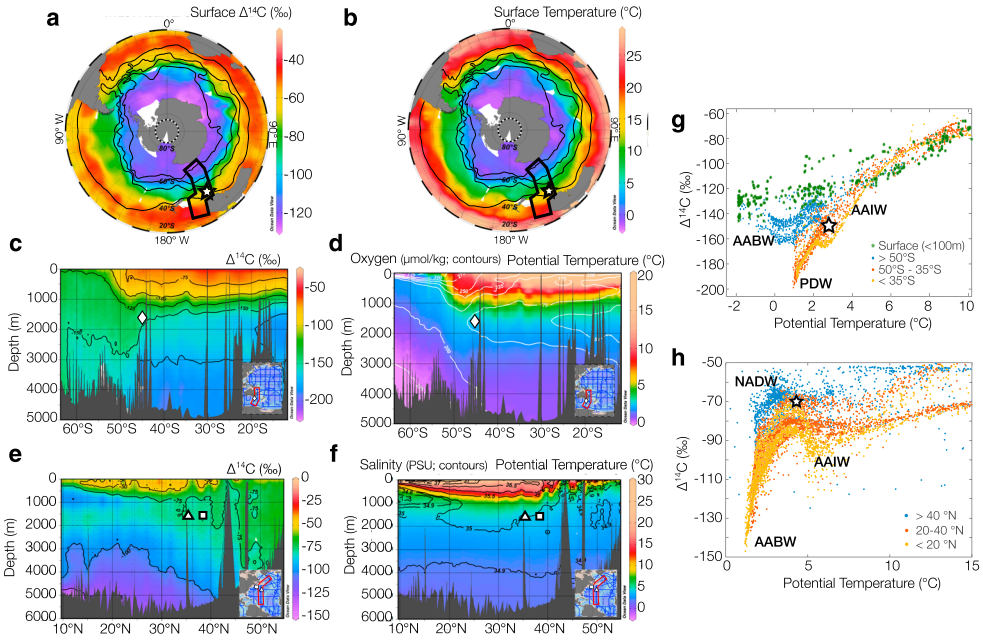

Figure 2. Modern hydrography from the Southern Ocean and North Atlantic. Surface plots of $\Delta^{14}C$ (NAT14C variable from the Global Ocean Data Analysis Project (GLODAP) database; a) and temperature (b) with front positions marked (Key et al., 2004; Orsi et al., 1995). Sections of Southern Ocean $\Delta^{14}C$ (c) and potential temperature with oxygen contours (d). Sections of North Atlantic $\Delta^{14}C$ (e) and potential temperature with salinity contours (f). (g) Crossplot of modern Southern Ocean potential temperature and $\Delta^{14}C$ from section in panels (c) and (d). Data are segregated by depth and latitude and sample location is marked with a star. (h) Crossplot of modern North Atlantic potential temperature and $\Delta^{14}C$ from section in panels (e) and (f). Data are segregated by latitude, and sample location is marked. AAIW = Antarctic Intermediate Water; AABW = Antarctic Bottom Water; PDW = Pacific Deep Water; NADW = North Atlantic Deep Water.

and 2b; Key et al., 2004). These horizontal gradients at the surface are transferred into vertical gradients as water subducts along sloping isopycnals in the Southern Ocean (Figure 2c). At intermediate water depths north of the Antarctic Circumpolar Current, this water mass distribution leads to two primary ways of generating signals in temperature and radiocarbon. The first mechanism, which can occur on short (decadal to centennial) timescales, is the movement of fronts at the surface in the Southern Ocean. Temperature and radiocarbon values are aligned with the major Southern Ocean fronts, so even without a change in circulation, frontal movement could change the initial value of water at the ventilation region, which would in turn change the value at depth. Alternatively, rearrangement of water masses (such as a switch from "figure-eight" to "two-cell" circulation) could change the amount of PDW influence at intermediate depths, which is predominantly characterized by old radiocarbon values and low oxygen concentrations (Figures 2c and 2d). These mechanisms can be separated by combining temperature and radiocarbon data and visualized on a crossplot of modern $\Delta^{14}C$ and potential temperature data (Figure 2g). Surface data are represented by green stars and have a fairly shallow slope in $\Delta^{14}C$ versus temperature space. Variability driven by frontal movement at the surface should follow this shallow slope. Changes in the amount of PDW reaching our site would drive steeper trends. In the modern ocean, our sample depth range is occupied by Upper Circumpolar Deep Water (UCDW), which is characterized by its oxygen minimum and influenced by the return of PDW to the Southern Ocean (Figure 2d). Our sample location is marked by a star and has a modern temperature of ~2.3 ° C and a modern $\Delta^{14}C$ value of approximately −150‰ (Figure 2g).

In the modern North Atlantic, radiocarbon values are much younger than the Southern Ocean due to the influence of well-ventilated NADW. The influence of young NADW is strongest north of 40° N but persists south of 10° N between ~1,000 and 3,000 m. This well-ventilated NADW endmember lies between older AAIW and AABW (Figure 2e). In the $\Delta^{14}C$-temperature crossplot, there are three endmembers in the deep ocean: NADW, AAIW, and AABW. The AAIW endmember is most prominent south of 20° N (Figure 2h). Our sample location sits between the NADW and AAIW endmembers with a modern temperature of ~4 °C and a modern $\Delta^{14}C$ value of approximately −70‰ (Figure 2h). Changes in NADW flux would primarily

affect the radiocarbon value of intermediate water. Prolonged decreases in NADW formation could lead to decreases in radiocarbon and increases in temperature at intermediate depth, due to heat diffusion across the main thermocline at midlatitudes (Marcott et al., 2011). Changes in the initial age of NADW, due to increased sea ice extent, for example, could also influence our site.

2. Methods

Deep-sea corals used in this study were collected from seamounts south of Tasmania (43–47° S, 144–152° E) during cruise TN-228 in 2008–2009 on the R/V Thompson using the remotely operated deep submergence vehicle JASON, from the New England Seamounts in the Northwest Atlantic (38–39°N, 50–61°W) during cruise AT7-35 in 2003 on the R/V Atlantis using human-occupied deep submergence vehicle ALVIN, and from the Corner Rise Seamounts in the Northwest Atlantic (35–36° N, 49–52° W) during cruise RB05-08 in 2005 on the R/V Ronald H. Brown using the remotely operated deep submergence vehicle HERCULES. During these cruises, around 16,500 deep-sea corals were collected from between 898 and 2,395 m in the Southern Ocean and 1,098 and 2,763 m in the North Atlantic. All corals used for the construction of this time series were members of the scleractinian azooxanthellate species *Desmophyllum dianthus*. The Southern Ocean time series presented here encompasses 32 samples from 1,440–1,900 m with 70% of samples from between 1,500 and 1,700 m. Three of these corals were subsampled for top-bottom ^{14}C and temperature measurements. The North Atlantic radiocarbon time series presented here consists of 38 samples from 1,176–1,751 m with 75% of samples from between 1,494 and 1,713 m, and the clumped isotope time series is from subset of these samples. It consists of 19 corals from between 1,494 and 1,751 m.

2.1. U/Th and Radiocarbon Dating

Previously, these samples had all been age screened at the NOSAMS lab at Woods Hole and the KCCAMS lab at UC Irvine (Hines et al., 2015; Thiagarajan et al., 2013) following the methods of Burke et al. (2010) and Bush et al. (2013), respectively (see Figure S1 in the supporting information). This age screening informed the selection of corals for further U/Th and high-precision radiocarbon dating (Hines et al., 2015, and references therein). Uranium and thorium were measured on the Neptune MC-ICPMS at Caltech using established methodologies (Hines et al., 2015). High-precision radiocarbon dating was done at the KCCAMS lab at UC Irvine, and background correction for the Southern Ocean samples were made based on replicate samples ($n = 8$) of a radiocarbon dead deep-sea coral ($F_m = 0.0034 \pm 0.0007$) with a U/Th age of 205,000 ± 3,000 years (Hines et al., 2015). North Atlantic data were measured in two separate blocks and corrected using the same radiocarbon dead coral, based on measurements made during those two measurement periods ($F_m = 0.0040 \pm 0.0013$ and $F_m = 0.0029 \pm 0.0010$, respectively). Combined U/Th ages and radiocarbon dates allow for the reconstruction of water $\Delta^{14}C$:

$$\Delta^{14}C = \left(\frac{e^{-^{14}\text{C age/Libby Mean Life}}}{e^{-\text{U/Th age/True Mean Life}}} - 1 \right) \times 1,000\,, \tag{1}$$

where the Libby Mean Life is 8,033 years and the True Mean Life is 8,266 years (Stuiver & Polach, 1977). This $\Delta^{14}C$ value corrects for the time elapsed since each coral sample grew, thereby extracting the $\Delta^{14}C$ value of the water it grew in, relying on the assumption that both the carbon isotope system and the U/Th isotope system have remained closed. In order to understand past changes in ocean circulation, it is more useful to compare reconstructed coral $\Delta^{14}C$ to the $\Delta^{14}C$ value of the contemporaneous atmosphere. This is done by converting the coral $\Delta^{14}C$ into epsilon notation:

$$\epsilon^{14}C = \left(\left[\frac{\frac{\Delta^{14}C_{sample}}{1000} + 1}{\frac{\Delta^{14}C_{atm}}{1000} + 1} \right] - 1 \right) \times 1,000\,. \tag{2}$$

Epsilon is a more correct measure of past ocean circulation changes than $\Delta\Delta^{14}C$ because it takes into account changes in atmospheric $\Delta^{14}C$ value itself (Soulet et al., 2016). It is therefore the parameter that stays constant (for sufficiently slow ^{14}C production changes) if ocean circulation does not change.

2.2. Clumped Isotope Measurements

Clumped isotope temperatures were measured on a dual-inlet Finnegan MAT-253 IRMS connected to an automated carbonate sample preparation line (Ghosh et al., 2006; Passey et al., 2010). Deep-sea corals were first cut and physically cleaned to remove any ferromanganese crusts, which can skew measurements of the

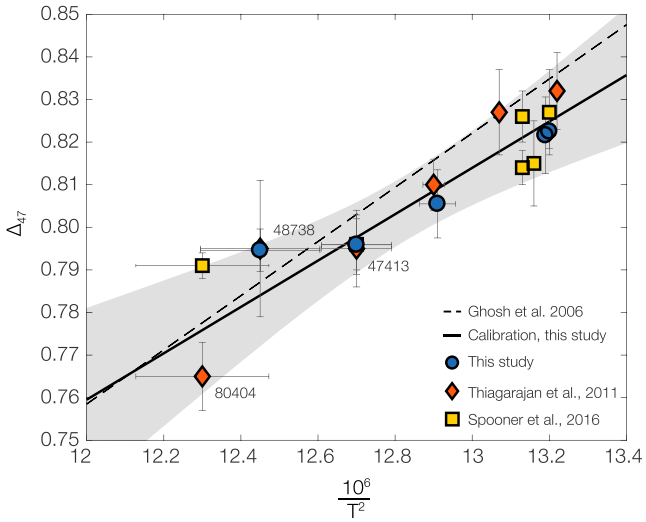

Figure 3. Modern *Desmophyllum dianthus* coral clumped isotope calibration. Average measured Δ_{47} (with 1σ SE) plotted versus growth temperature. Measurements made by Thiagarajan et al. (2011) and Spooner et al. (2016) are plotted as well. Δ_{47} values from Thiagarajan et al. (2011) and Spooner et al. (2016) are corrected to measurements from this study using overlapping samples. Growth temperatures were determined using the Ocean Data View software and the GLODAP database (Key et al., 2004), and three samples with large growth temperature error bars are labeled (47413, 48738, and 80404, discussed in text). York regression line for samples run at Caltech (excluding Spooner et al., 2016, data which were run at the Woods Hole Oceanographic Institution) is plotted in solid line with 90% confidence interval. York regression line for Ghosh et al. (2006) data is plotted in dashed line (Huntington et al., 2009; Dennis et al., 2011).

bulk coral (Thiagarajan et al., 2014, 2011). Then samples were powdered for analysis, and approximately 8 mg of powder was used for each measurement. Carbonates were digested in 105% phosphoric acid at 90 ° C and purified in an automated line. Water was removed by passing gas through an ethanol/dry ice slush, and CO_2 was trapped in liquid nitrogen. Other contaminants were removed by passing the CO_2 gas through a Porapak Q 120/80 mesh GC column at −20 ° C, then the resulting gas was transferred to the mass spectrometer. In the mass spectrometer, beams corresponding to masses 44–49 were simultaneously measured and used to calculate Δ_{47}, Δ_{48}, Δ_{49}, $\delta^{13}C$, and $\delta^{18}O$. R^{47} is defined as the sum of the mass-47 isotopologues ($^{17}O^{13}C^{17}O$ + $^{17}O^{12}C^{18}O$ + $^{16}O^{13}C^{18}O$) divided by the mass-44 isotopologue ($^{16}O^{12}C^{16}O$). Δ_{47} is defined relative to the stochastic distribution of isotopologues for a given isotopic composition:

$$\Delta_{47} = \left(\left[\frac{R^{47}_{\text{measured}}}{R^{47}_{\text{stochastic}}} - 1 \right] - \left[\frac{R^{46}_{\text{measured}}}{R^{46}_{\text{stochastic}}} - 1 \right] - \left[\frac{R^{45}_{\text{measured}}}{R^{45}_{\text{stochastic}}} - 1 \right] \right) \times 1,000 \,. \tag{3}$$

Measurements at mass 48 were used to monitor for hydrocarbon contamination. Each aliquot of gas was measured for eight acquisitions, which consisted of seven cycles of sample-standard comparison with an integration time of 26 s.

Raw Δ_{47} values were corrected for nonlinearity and fragmentation within the mass spectrometer, converted into the "absolute reference frame," and corrected for acid bath digestion temperature (Dennis et al., 2011; Huntington et al., 2009; Passey et al., 2010). Typical errors on a single Δ_{47} measurement are ~0.01‰, which corresponds to ~2 ° C. Each deep-sea coral was measured 4–10 times to increase precision, and replicate measurements were averaged to make a single Δ_{47} value. Error for these averages are reported as the standard error of averaged replicate measurements.

2.3. Conversion of Δ_{47} to Temperature

Average Δ_{47} values were converted to temperature using a new modern coral calibration derived from samples run at Caltech. Previous modern deep-sea coral calibration studies by Thiagarajan et al. (2011) and Spooner et al. (2016) concluded that deep-sea coral Δ_{47} values were not inconsistent with the Ghosh calibration in the absolute reference frame (Dennis et al., 2011); however, Spooner et al. (2016) also concluded

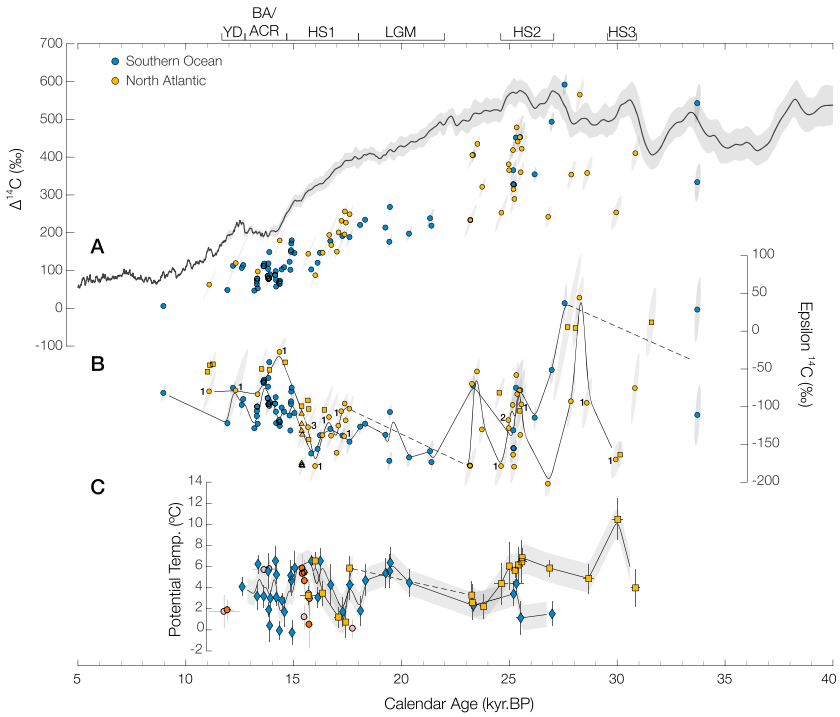

Figure 4. Summary of all deep-sea coral results. (a) $\Delta^{14}C$ records from the North Atlantic and Southern Ocean. Coral $\Delta^{14}C$ values are plotted with 1σ error ellipses that take into account correlated U/Th age and ^{14}C date error. IntCal13 atmospheric $\Delta^{14}C$ record is also plotted for reference (Reimer et al., 2013). (b) North Atlantic and Southern Ocean $\Delta^{14}C$ data converted into Epsilon ^{14}C. Small numbers adjacent to North Atlantic $\epsilon^{14}C$ points indicate samples that failed either the ^{232}Th and/or $\delta^{234}U_i$ criterion (see Tables S4 and S5). North Atlantic data from Robinson et al. (2005), yellow squares; Eltgroth et al. (2006), yellow squares; Thiagarajan et al. (2014), yellow diamonds; and Adkins et al. (1998), yellow triangles, are also included. (c) Clumped isotope temperature records for the North Atlantic and Southern Ocean. Data from Thiagarajan et al. (2014) are also included (dark orange circles are from 1,500 to 2,000 m, and light pink circles are from 1,000 to 1,500 m). Measured Δ_{47} values are converted to temperature using our new *Desmophyllum dianthus* coral calibration, and temperatures are converted to potential temperature using each coral's collection depth and latitude. In order to better visualize long-term trends in the data, North Atlantic and Southern Ocean Epsilon ^{14}C and temperature records were interpolated at 10-year resolution and smoothed using a 500-year Gaussian filter (black lines). Error envelope in (c) is average 1SE temperature error for North Atlantic and Southern Ocean.

that each deep-sea coral species exhibits slightly different behavior from the others, and they therefore recommended species-specific clumped isotope calibrations for future studies. While our data are also broadly consistent with the Ghosh calibration, we feel that creating a new species-specific deep-sea coral calibration for *Desmophyllum dianthus* focusing on the relevant temperature range will yield more accurate temperature reconstructions. We only include measurements made at Caltech, since it has been established that Δ_{47} measurements made in different labs are not always consistent (Defliese et al., 2015; Fernandez et al., 2017; Kelson et al., 2017). Recent clumped isotope community discussions have also concluded that carbonate standard correction dramatically improves long-term and interlab reproducibility (Bernasconi et al., 2018). Therefore, we have used overlapping samples 47413 and 48738 to correct samples run by Thiagarajan between 2008 and 2015 to our samples run in 2017. Modern temperatures for the samples measured were determined using the 3-D interpolation function in Ocean Data View (Key et al., 2004). For three of the samples (47413, 48738, and 80404), data were either sparse at the collection location or the sample grew near strong temperature gradients in the water column, so growth temperatures and growth temperature errors were estimated by hand using water column profile data. Corrected samples are plotted in Figure 3 with the york regression line and 95% confidence interval. For reference, carbonate corrected *Desmophyllum dianthus* samples from Spooner et al. (2016) are also plotted but were not used for the york regression (Table S1).

3. Results

3.1. Clumped Isotope Temperatures

Deep-sea coral samples were measured between four and nine times each. Temperature errors ranged from 0.5 to 2.6 ° C (1 SE), with an average value of 1.2 ° C (Tables S2 and S3). All three Southern Ocean corals that were subsampled for top-bottom temperature measurements differed outside of error. In addition to the 32 Southern Ocean and 19 North Atlantic fossil deep-sea corals, one additional Southern Ocean coral that had been collected alive was measured. It was collected from the same location as deep-sea coral standard LB-001. Replicate measurements of this sample, SH-A008-S5, agree within 2σ SE with replicate measurements of LB-001 for the weeks that they were measured together.

North Atlantic and Southern Ocean clumped isotope temperature records are shown in Figure 4c (all replicates with averages and standard errors are in Figure S5). In the North Atlantic, there is some temperature variability early in the record, between 29 and 31 ka, with one extremely warm sample at 30 ka. Then, after a slight rise in temperature between 28 and 25 ka, there is a drop in temperature during Heinrich Stadial 2 (~24–27 ka). In Southern Ocean, there is also a drop in temperature during Heinrich Stadial 2, although it is not as large or abrupt and not outside error bars. There is a large gap in the North Atlantic record during the LGM, between 17.6 and 23.3 ka. During the LGM, Southern Ocean temperatures rise, peaking at ~19 ka, then drop with some variability through ~17 ka. North Atlantic temperatures mirror this drop and then both records rise through the middle of Heinrich Stadial 1, with some variability. During the Antarctic Cold Reversal (ACR; ~13–14.7 ka), Southern Ocean temperatures show a high degree of variability on short timescales, reaching both the coldest and nearly the warmest temperatures observed in the whole Southern Ocean record.

3.2. North Atlantic U/Th and Radiocarbon Dates

In addition to the 44 Southern Ocean corals previously radiocarbon dated, including eight that were subsampled (see Hines et al., 2015), an additional 52 North Atlantic corals were U/Th dated (Table S4), and 38 of these samples were also radiocarbon dated (Table S5). U/Th dates were assessed based on two criteria: ^{232}Th concentration, which increases age error due to uncertainty in the initial ^{230}Th/^{232}Th ratio, and the initial δ^{234}U value (where $\delta^{234}U_i = \delta^{234}U_{meas}e^{\lambda t}$), which should be within error of the marine δ^{234}U value and assesses whether or not the sample has behaved like a closed system. We impose a ^{232}Th concentration cutoff value of 2,000 ppt and assign a range of acceptable $\delta^{234}U_i$ values following IntCal09 (Reimer et al., 2009): 147 ± 7‰ for samples younger than 17 ka and 141.7 ± 7.8‰ for samples older than 17 ka. A much higher fraction of North Atlantic U/Th dates had high ^{232}Th compared to the Southern Ocean. Of the 52 North Atlantic samples, 22 had ^{232}Th concentrations higher than the cutoff value of 2,000 ppt (compared to 14 out of 103 for the Southern Ocean). Two samples failed the $\delta^{234}U_i$ criterion, and three additional samples failed both criteria.

In general, we aimed to radiocarbon date samples with low ^{232}Th in order to minimize age uncertainties; however, due to the large number of samples with high thorium, we radiocarbon dated 11 samples with >2,000 ppt ^{232}Th, one sample that missed the $\delta^{234}U_i$ criterion, and one sample that missed both. Of the samples with >2,000 ppt ^{232}Th, all but three had <3,000 ppt ^{232}Th (the other three had 5,070, 3,150, and 3,100 ppt). Of the samples that failed the $\delta^{234}U_i$ criterion, one at 15.7 kyr missed by 0.16‰, and the other at 25.0 kyr missed by 3.14‰. Open-system behavior, as indicated by the $\delta^{234}U_i$ value, has more potential to systematically bias ages than high ^{232}Th; however, both samples that miss the $\delta^{234}U_i$ criterion agree with adjacent samples that are more well behaved. Average relative radiocarbon age errors were 4.1‰ for samples younger than 15,000 ^{14}C-years, 4.7‰ for samples between 15,000 and 20,000 ^{14}C-years, 7.4‰ for samples between 20,000 and 25,000 ^{14}C-years, and 11.2‰ for samples older than 25,000 ^{14}C-years. These errors are controlled by variability in the blank for ^{14}C-dead deep-sea corals, which is larger than that of calcite.

North Atlantic Δ^{14}C values are generally in agreement with Southern Ocean Δ^{14}C values (Figure 4a). In the early part of the record, before the start of the LGM (at ~22 ka), there is a large amount of variability in Δ^{14}C value, and samples fall fairly close to the atmosphere, with two Southern Ocean samples and one North Atlantic sample lying above the IntCal13 atmospheric Δ^{14}C curve. There is a 5,600-year gap in the North Atlantic record during the LGM between 17.6 and 23.2 ka. During this time period, the Southern Ocean data generally parallel the atmosphere with one abrupt jump at ~19 ka. Starting at 17.6 ka, there is a well-resolved drop in North Atlantic Δ^{14}C of ~160‰ over 1,600 years. There is also a drop in Southern Ocean Δ^{14}C between 15.8 and 16.7 ka, but it is shallower in slope. There are 43 Southern Ocean Δ^{14}C points

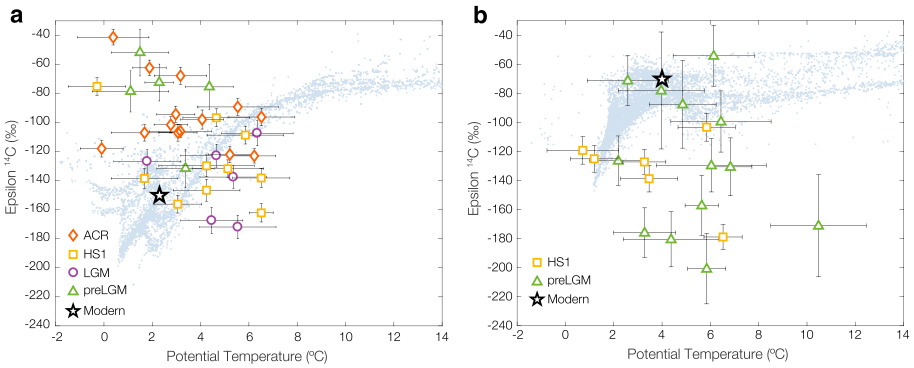

Figure 5. Crossplots of Southern Ocean (a) and North Atlantic (b) radiocarbon and temperature data. Radiocarbon data are converted into ϵ^{14}C, and temperatures are converted into potential temperature. Time periods are "pre-LGM" (>22 ka), "LGM" (18–22 ka), "HS1" (14.7–18 ka), and "ACR" (<14.7 ka). Modern potential temperature and radiocarbon ("NAT14C") data from the GLODAP database are plotted in the background (Key et al., 2004). Modern value is marked with a black star.

younger than 15.1 ka, and they show a great deal of short-timescale variability, particularly during the ACR. There are only five North Atlantic samples younger than 16 ka, and they generally agree with the Southern Ocean data, except one sample at 14.4 ka that is very close to the atmosphere ($\epsilon^{14}C = -28‰$).

3.3. Radiocarbon and Temperature Crossplots

Compiled North Atlantic and Southern Ocean radiocarbon (converted into ϵ^{14}C) and potential temperature records are shown in Figures 4b and 4c, and crossplots of radiocarbon and potential temperature are shown in Figure 5 with modern data in the background and the modern sample location marked. In both the North Atlantic and Southern Ocean, fossil corals fall far outside the range of modern data. For the Southern Ocean, LGM and HS1 samples (see figure caption for age ranges) are warmer and similar in age to the modern and ACR, and pre-LGM samples are much younger and slightly colder. For the North Atlantic, there is a wide range of temperature and radiocarbon for all the data, and samples tend to be much older than the modern. Unlike the Southern Ocean, pre-LGM and HS1 samples are interspersed in the North Atlantic, but there is a larger range of radiocarbon for the pre-LGM samples.

4. Discussion

4.1. The Separate Strengths of Deep-Sea Corals and Foraminifera as Archives of Past Climate Change

Information derived from sediment cores has shaped our understanding of the past ocean. Cores have been taken from many places across the global ocean, and they offer continuous information about ocean conditions at a specific location. By coring along bathymetric features, multiple sediment cores at different depths can be used to understand changes in vertical water mass structure over time. However, despite the importance of sediment cores for the field of paleoceanography, the impression they give of the ocean's time evolution is inherently biased. Bioturbation mixes the upper part of the sediment column when bottom waters are oxygenated, causing signals recorded in the sediments to be smoothed. Additionally, due to sample size constraints, geochemical measurements often require many individual foraminifera, adding another averaging step between the original signal and the final data. In contrast, the real ocean is highly variable both spatially and temporally. Modern physical oceanography has emphasized the important role that eddies play in ocean dynamics, and recent monitoring studies have highlighted the variability of the overturning circulation on subannual timescales, which can be order 10 Sv (e.g., Bryden et al., 2009).

Deep-sea corals come from a much smaller number of locations, and coral populations are not continuous in depth and time. The depth range and abundance of corals is dictated by environmental conditions, predominantly in situ oxygen and carbonate ion concentrations (Thiagarajan et al., 2013). Corals have the advantage of precise age control via U/Th dating and large sample size, which enables multiple geochemical measurements to be made on a single individual. *Desmophyllum dianthus*, the species we have used in this study, grow for several decades to about 100 years (Adkins et al., 2004), and because they are unbioturbated, they are much more sensitive to the variability that exists in the ocean. Deep-sea corals are like tiny moored

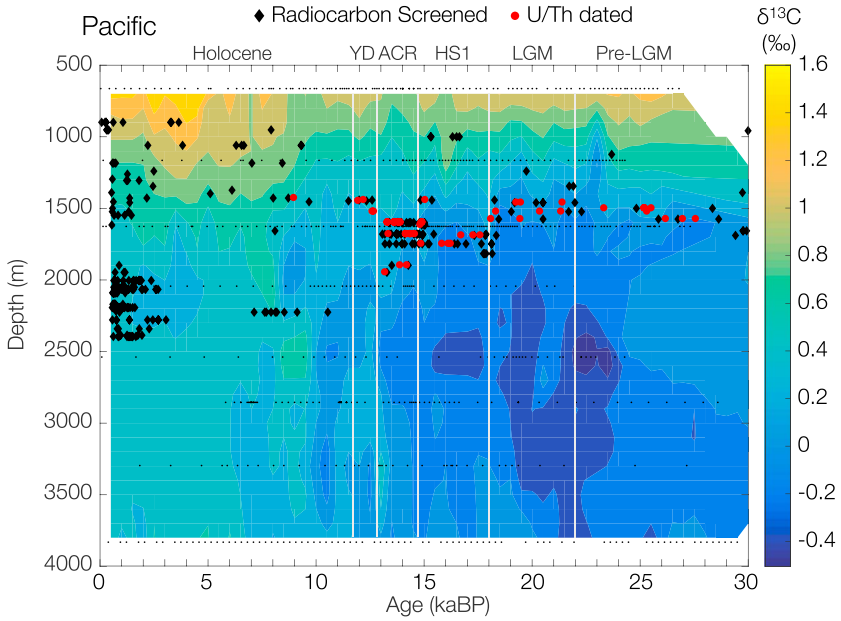

Figure 6. Response of deep-sea coral population to deep Southern Indo-Pacific ocean evolution across the deglaciation. δ^{13}C measurements from a transect of sediment cores near New Zealand are contoured in depth and time (Sikes et al., 2016). Black dots mark depths and ages of benthic δ^{13}C measurements. Ages and depths of Tasmanian deep-sea coral population are overlaid (black diamonds are radiocarbon-screened ages, and red circles are U/Th dates; Hines et al., 2015.)

CTDs—fixed at a specific location and recording the variable water masses that bathe them. If they are living near a sharp water property gradient in the ocean, they should record more variable signals compared to times when they live in the middle of a homogenous water mass. Like moored CTDs in the modern ocean, the time series data they record is often difficult to interpret (much like the deep-sea coral time series data in Figure 4), but by making crossplots it is possible to visualize the different endmembers that are present at different times (Figure 5).

Our deep-sea corals from south of Tasmania are very close to a depth transect of sediment cores from around New Zealand, which span over 3,000 m of the water column and record changes in water mass structure across the LGM and deglaciation (Sikes et al., 2016). This allows us to directly compare deep-sea coral and foram-derived records across the last 30 kyr. Figure 6 shows the evolution of the Indo-Pacific δ^{13}C depth-structure across the deglaciation (Sikes et al., 2016) and how the deep-sea coral population responds to ocean changes across this same time period (black diamonds are reconnaissance radiocarbon dates, and red circles are U/Th dates; Hines et al., 2015). Taking these two independent data sets together, it is clear that the coral population is responding to aspects of deep ocean chemistry that are also reflected in the δ^{13}C data. Between 30 ka and the end of the ACR, the maximum depth of the corals nearly follows a single δ^{13}C contour. The corals used for the construction of our radiocarbon and temperature records (red circles) sit along a strong tracer gradient, and it is therefore unsurprising that they record highly variable signals across this time interval. We will use this comparison between the Indo-Pacific δ^{13}C depth transect and the Tasmanian deep-sea coral data to contextualize our radiocarbon and temperature data across the late glacial and deglaciation. We will use crossplots of different time slices to see beyond the variability in our time series data and identify different water mass endmembers that are present at different times (Figure 7).

4.2. Evolution of Circulation Across the Deglaciation

4.2.1. Pre-LGM: 31–22 ka

Across the end of the last glacial period, Southern Ocean deep-sea coral data lie at the interface between a deep δ^{13}C-depleted water mass and a shallow enriched water mass (Figure 6). In the time immediately preceding the LGM, measured radiocarbon values are much younger than the modern ocean value (Figure 7a). In the modern ocean, water between 1,400 and 1,600 south of Tasmania acquires its old radiocarbon signature of approximately −150‰ from a mixture of two main sources: old PDW (see Figures 2c, 2d, and 2g), which lies deeper and to the north and is characterized by its low O_2 concentrations, and younger AAIW

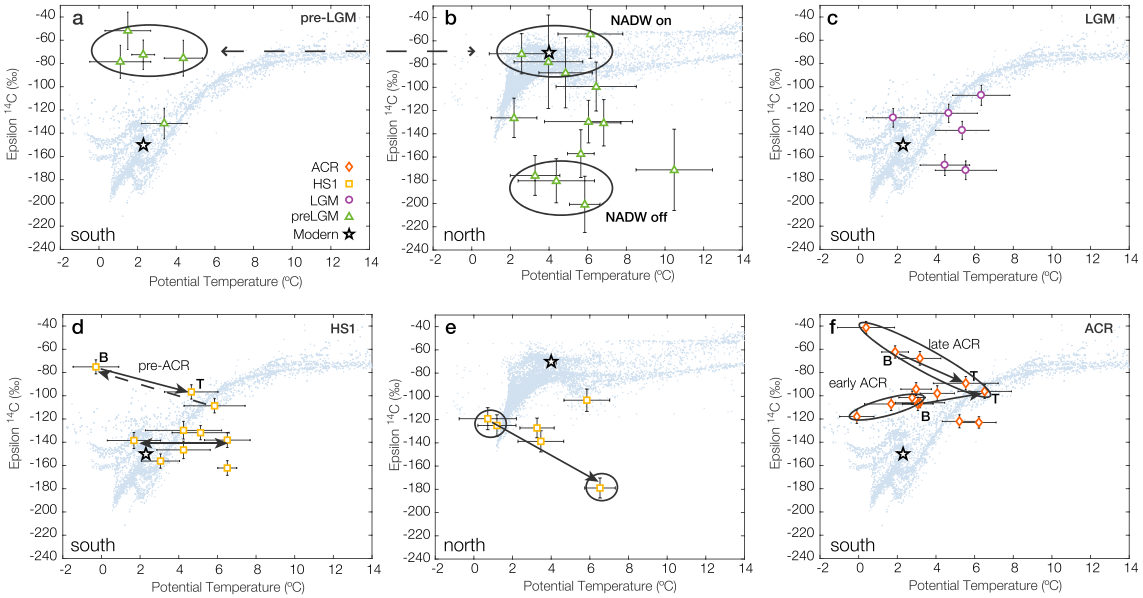

Figure 7. Crossplots of radiocarbon and temperature from the North Atlantic and Southern Ocean from different time slices across the late glacial. In all panels, modern potential temperature and radiocarbon data are plotted in the background (Key et al., 2004). Southern Ocean (a) and North Atlantic (b) data from the pre-LGM time slice (>22 ka). Dashed line connects a similar endmember seen in both the north and south and North Atlantic Deep Water (NADW) on and off endmembers are circled. (c) Southern Ocean data from the Last Glacial Maximum (LGM; 18–22 ka). Southern Ocean (d) and North Atlantic (e) data from Heinrich Stadial 1 (14.7–18 ka). Arrows in panel (d) show direction of variability in early HS1 and "pre-ACR" intervals. Arrow in panel (e) marks North Atlantic trend from colder more ventilated waters early in HS1 to warmer, radiocarbon-depleted waters late in HS1. (f) Southern Ocean data from the Antarctic Cold Reversal (<14.7 ka). Circles mark data from the beginning and end of this time interval. In panels (d) and (f), "T" and "B" labels indicate top and bottom subsamples of three individual corals, and solid arrow indicates direction of change over the lifetime of the coral.

(Figure 2g). In the modern Southern Ocean, this water mass would best be described as Upper Circumpolar Deep Water. In the ocean interior, water acquires a light stable carbon isotope signature, as it ages due to addition of respired ^{13}C-depleted organic matter. While this should generally accompany a decrease in radiocarbon value as the result of decay, there is a much larger dynamic range for radiocarbon (~250‰) compared to δ^{13}C (~2‰). Radiocarbon and ^{13}C have different boundary conditions, which can lead to different mixing relationships between the two tracers. These different boundary conditions are driven in part by the fact that δ^{13}C has a minimum value and a maximum vertical gradient, which is driven by the efficiency of the biological pump. Once this maximum gradient is achieved, δ^{13}C is no longer sensitive to changes in circulation, while ^{14}C can continue to decay in the interior. Despite these caveats, we expect that the radiocarbon-young water our samples record is the shallow δ^{13}C-enriched water mass. Our data indicate that either PDW was more isolated from our samples, perhaps because it was deeper in the water column, that initial radiocarbon ages of our samples were younger, or that there was some combination of both.

In the North Atlantic, there is evidence for a water mass with a very similar radiocarbon value to that which is found south of Tasmania (Figure 7b). This young endmember overlaps with the modern North Atlantic radiocarbon and temperature value and is likely indicative of strong NADW formation. A second North Atlantic endmember, which is much more depleted in radiocarbon (more negative ϵ^{14}C), is likely the result of weakened NADW formation. Before the start of the LGM there is evidence from several proxies that there were multiple abrupt changes in ocean circulation. Dansgaard-Oeschger events 2–4 (Figure 1b) and Heinrich events 2 and 3 (Figure 1, dark gray bars) occurred during this time interval and were associated with changes in atmospheric (Figure 1f) and ocean circulation (Figure 1e). From the crossplot (Figure 7b) it is difficult to say whether the NADW on and off endmembers have different temperatures given the scatter in the data and error bars on individual data points; however, there are much clearer trends in the time series of temperature from this time interval (Figure 4c). In particular, we see a coherent decrease in temperature during Heinrich Stadial 2 (26–23 ka) in the North Atlantic coincident with a decrease in ϵ^{14}C. This pattern is somewhat unexpected given evidence from Pa/Th records for a decrease in overturning strength at this time (Figure 1e; Lippold et al., 2009), which should result in decreased radiocarbon values and increased

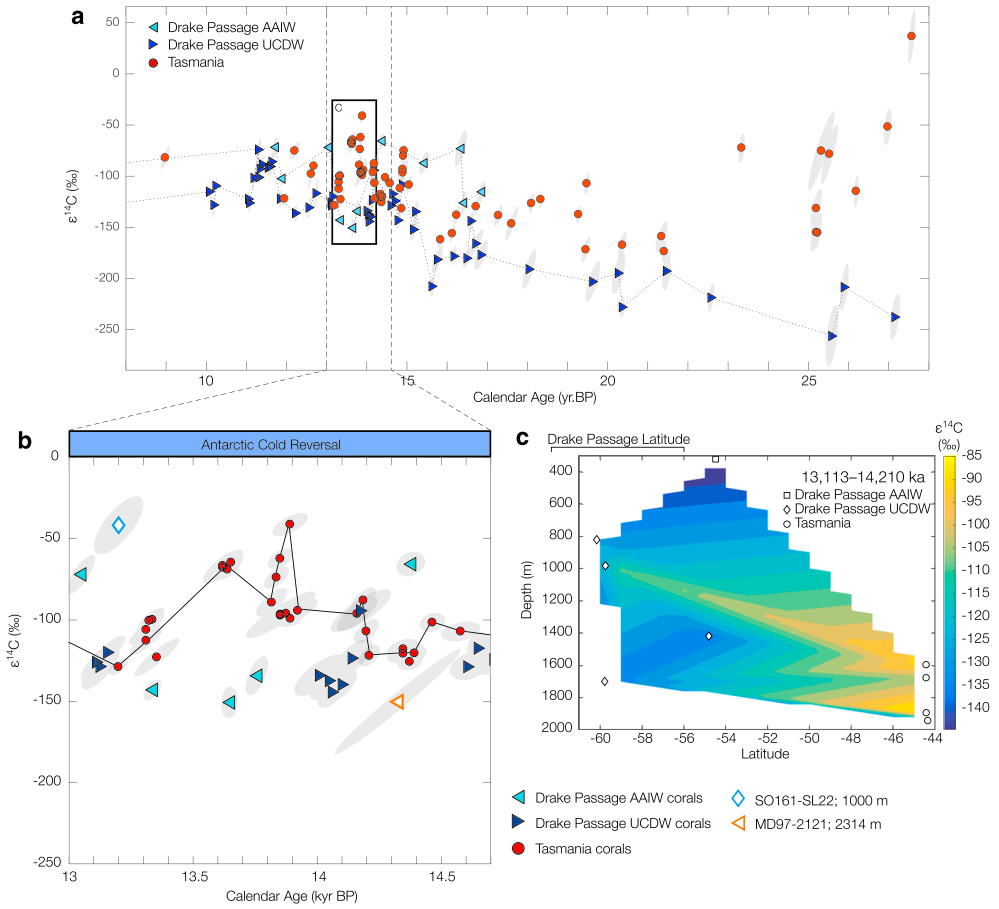

Figure 8. Comparison of radiocarbon records from the Southern Ocean. (a) Tasmanian radiocarbon data with Drake Passage Antarctic Intermediate Water (AAIW; light blue left-facing triangles) and UCDW (dark blue right-facing triangles) data (Burke & Robinson, 2012; Chen et al., 2015). (b) Comparison of Antarctic Cold Reversal deep-sea coral and benthic foram data from the Chilean Margin (light blue open diamonds; De Pol-Holz et al., 2010), Drake Passage (as in panel a), Tasmania (red circles and solid line; Hines et al., 2015), Chatham Rise (orange open left-facing triangles; Skinner et al., 2015). (c) Depth-latitude contour plot of deep-sea coral ϵ^{14}C data from boxed time period in panel (a).

temperatures at intermediate depths (Marcott et al., 2011). One possible explanation for the discrepancy is the difference in boundary condition moving into the LGM versus moving out.

4.2.2. Last Glacial Maximum: 22–18 ka

During the LGM, there is an enhancement of the deep Indo-Pacific δ^{13}C minimum and an increase in the δ^{13}C gradient in the water column above where our deep-sea coral samples lie (Figure 6). These changes are accompanied by a decrease in the radiocarbon age of Tasmanian samples (Figure 7c), indicating that they are more strongly influenced by the deep δ^{13}C-depleted water and more isolated from the shallow δ^{13}C-enriched water. Despite the strongly depleted δ^{13}C signature at depth, Tasmanian radiocarbon values are similar to the modern value and agree with Drake Passage Upper Circumpolar Deep Water (UCDW) samples from between 22 and 19 ka (Figure 8a; Burke & Robinson, 2012; Chen et al., 2015).

Deep-sea coral temperatures are warm during this interval, with peak temperatures of approximately 6 ° C at 19 ka. The presence of warm water at ~1,600 m south of Tasmania reinforces the hypothesis that stratification at the LGM was dominated by salinity differences rather than temperature differences (Adkins, 2002). The Tasmanian deep-sea coral temperature peak immediately follows the peak in Southern Hemisphere summer insolation (Figures 1a and 4c), indicating that while continental ice sheets respond to Northern Hemisphere summer insolation (giving glacial cycles their characteristic pacing) Southern Ocean intermediate water temperatures are more sensitive to local insolation. Antarctic ice cores also begin to warm around this time, exhibiting similar sensitivity to local insolation (Figure 1c; WAIS Divide Project Members, 2013).

4.2.3. Heinrich Stadial 1: 18–14.7 ka

In the early part of Heinrich Stadial 1 (between ~18 and 16 ka), Tasmanian deep-sea coral samples occupy a very similar region of radiocarbon-temperature space to the LGM (Figures 7c and 7d), although we observe more temperature variability in the time series (Figure 4c). While these samples come from slightly deeper in the water column, they still follow a similar δ^{13}C contour (Figure 6). The deep δ^{13}C minimum that developed during the LGM begins to deteriorate at the beginning of HS1 but is still present until 16 ka. At around 16 ka, the deep δ^{13}C minimum breaks down abruptly (particularly between ~1,500 and 2,000 m), potentially driven by changes in the ocean-atmosphere system in response to Heinrich Event 1 (Figures 1d and 1f). Tasmanian samples also abruptly get younger at this time (Figure 7d; "pre-ACR" samples).

Records from the North Atlantic indicate that Heinrich Stadial 1 was characterized by reduced NADW formation (Figure 1e) and the persistence of cold conditions in the region (Figure 1b). Our North Atlantic deep-sea coral data also show evidence for reduced NADW formation. As has been previously observed and modeled, decreased NADW formation leads to older radiocarbon ages and warmer temperatures in the intermediate-depth North Atlantic (Dokken et al., 2013; Liu et al., 2009; Marcott et al., 2011), since newly formed NADW represents a source of young cold water. In its absence, intermediate and deep waters stagnate and downward diffusion of heat in the subtropics causes warming at intermediate depths. This trend toward older and warmer water in the intermediate North Atlantic can be seen in the crossplot (Figure 7e) and our time series (Figures 4b and 4c).

4.2.4. Bølling-Allerød/ACR: 14.7–12.8 ka

By the ACR, much of the deep Indo-Pacific δ^{13}C minimum has dissipated (Figure 6); however, our Tasmanian deep-sea coral samples still sit at a strong tracer gradient that shifts in time and space. This spatial and temporal variability that can be seen in Figure 6 is also reflected in the highly variable Tasmanian radiocarbon and temperature records (Figure 4). From the radiocarbon-temperature crossplot, we see that Tasmanian corals fall in the same region that was occupied in the pre-LGM interval and by the three "pre-ACR" samples from HS1. Samples from the ACR time slice (Figure 7f) fall into two clusters, both of which are younger and colder than most of the data from the LGM and HS1. This could indicate that while salinity stratification during the late glacial and early deglaciation permitted warmer intermediate waters compared to the modern ocean, this salinity-dominated stratification is breaking down during the ACR.

Data for the early part of the ACR show a positive correlation between temperature and radiocarbon whereas data for the later part of the ACR show a negative correlation (circled and labeled in Figure 7f). Both clusters include one top-bottom ϵ^{14}C-temperature pair that trends in the direction of its respective data cluster. The early ACR cluster falls along the trend of surface data in the modern ocean (Figure 2g), indicating that observed variability is driven by the movement of surface fronts; however, the late ACR cluster falls along an opposing trend, mimicking the pre-ACR data (Figure 7D). The trend of the "pre-ACR" and "late ACR" data is somewhat unexpected given the pattern of modern radiocarbon and temperature data and the processes that should drive changes in intermediate water radiocarbon and temperature in the Southern Ocean (see Figures 2a, 2b, and 2g and accompanying text). Generally, radiocarbon and temperature are positively correlated at the surface of the Southern Ocean; however, the processes driving these two properties are quite different, and they have very different response times—temperature equilibrates quickly between the atmosphere and the ocean, whereas radiocarbon equilibrates much more slowly (since it requires isotopic equilibration with the whole surface DIC pool). Therefore, in times where the ocean is not at steady state, it is conceivable that the relationship between these tracers could change, especially if the ocean signal is driven by a change in the atmosphere, as is likely the case at the end of HS1.

Intermediate-depth radiocarbon records from across the Southern Ocean during the ACR show a somewhat coherent picture (Figure 8b). A single point from the Chatham Rise core MD97-2121 at 2314 m (Skinner et al., 2015) and a single point from the Chilean Margin core SO161-SL22 at 1,000 m (De Pol-Holz et al., 2010) lie during the ACR. The Chilean Margin sample should be in a similar water mass as the Drake Passage AAIW samples (although it is located much farther to the north), and indeed, they have similar ϵ^{14}C values. The Chatham Rise sample is constrained by tephra chronology, but there is still relatively large uncertainty in its ϵ^{14}C value. It has the oldest ϵ^{14}C value, although part of the error ellipse agrees with Drake Passage UCDW data. Age control is not a problem for U/Th-dated deep sea corals, allowing for a more direct comparison of the Tasmanian and Drake Passage data sets. In the modern ocean, the Tasmanian deep-sea corals lie in a similar water mass to the Drake Passage UCDW samples (although the Tasmanian samples are deeper

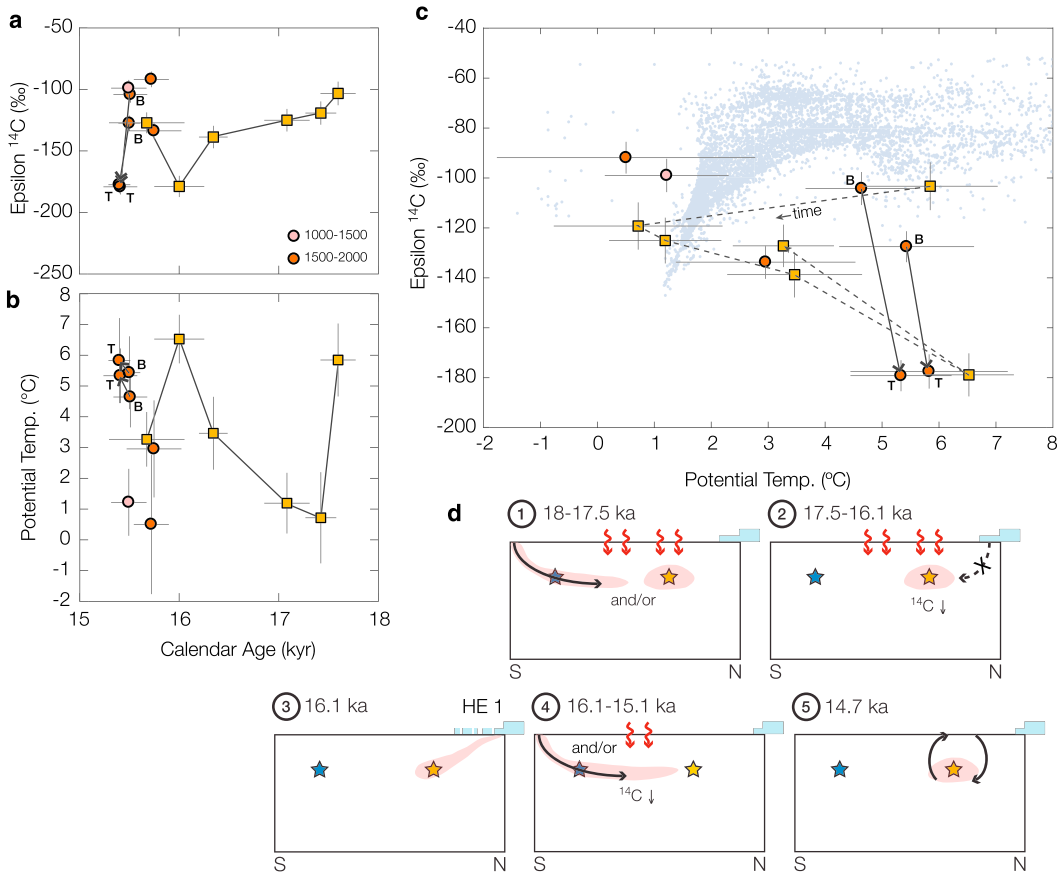

Figure 9. Comparison of deep-sea coral radiocarbon and temperature records during Heinrich Stadial 1. A) Radiocarbon data from this study (yellow squares) and Thiagarajan et al. (2014) (1000–1500 m in light pink circles and 1500–2000 m in dark orange circles). All data are plotted as ϵ^{14}C referenced to IntCal13 (Reimer et al., 2013). B) Clumped isotope temperature data with the same symbols as in A. N.B. Thiagarajan et al. (2014) sample at 17.7 ka not plotted because radiocarbon value was suspected to have been influenced by open system behavior. C) Crossplot of radiocarbon and temperature data from panels A and B. North Atlantic data from this study are connected by a dashed line representing the temporal evolution of the samples. Data from the modern North Atlantic are plotted in the background (Key et al., 2004). D) Schematic of radiocarbon and temperature sequence across HS1 (see text for description).

and further to the north), and these two records generally agree where there is overlap (Figures 8a and 8b; Burke & Robinson, 2012; Chen et al., 2015).

During the middle of the ACR, however, there is quite a confusing arrangement of water masses—the Drake Passage AAIW corals are older than our Tasmanian samples by around 70‰ (Figures 8a and 8b). This observation is difficult to explain given the modern arrangement of water in the Southern Ocean. One way to look at this time period is to plot all the Drake Passage and Tasmanian deep-sea corals from between 14.2 and 13.1 ka on a depth-latitude section with ϵ^{14}C contoured (Figure 8c). Figure 8C suggests that the signal of radiocarbon-young water is injected at depth, originating from the north (potentially the result of reinvigorated NADW formation at the start of the Bølling-Allerød). From this contour plot we also see that the oldest water is the shallowest, which suggests that exchange at the surface was reduced, perhaps as a result of expanded sea ice. We acknowledge, however, that this explanation is based on an implied steady state, zonally symmetric view of the Southern Ocean, averaging over ~1,000 years. The ocean is almost certainly not at steady state during this time, and it may not be appropriate to average over such large spatial and temporal scales.

One other explanation for the youngest Tasmanian sample in this interval (13.9 ka, $\epsilon^{14}C = -41‰$) is memory of the large drop in atmospheric Δ^{14}C that immediately precedes it. Epsilon values are calculated as the

offset from the contemporaneous atmosphere, but subsurface radiocarbon is a tracer that is strongly affected by past atmospheric radiocarbon values.

4.3. Comparison of North Atlantic Deep-Sea Coral Temperature Records

Recent work by Thiagarajan et al. (2014) proposed a mechanism for the initiation of the Bølling involving the buildup of heat at intermediate depths in the North Atlantic and then catastrophic release via thermobaric convection (Adkins et al., 2005; Su et al., 2016). They propose that warm intermediate waters, measured in the North Atlantic, originated from the Southern Ocean. For the times where there is overlap between our new deep-sea coral data and the Thiagarajan et al. (2014) record, both data sets agree; however, the only overlap is very early in the Heinrich Stadial (at ~18 ka) and at the end of the Heinrich Stadial (at ~15.7 ka). Between these times, our deep-sea coral data show a gradual rise in temperature (after an abrupt initial drop), whereas the Thiagarajan et al. (2014) record alone would imply that temperatures stayed cold and then abruptly warmed (Figures 4c and 9b).

In order to better understand the sequence of events during Heinrich Stadial 1 and reconcile the two data sets, we crossplot the data (Figure 9c). Examining all the data together, the crossplot shows three endmembers during this time: one young cold endmember, one young warm endmember, and one old warm endmember. Our oldest North Atlantic sample lies near the warm young endmember (which resembles modern AAIW in the equatorial Atlantic; see Figure 2f). The next samples record a shift to the cold young endmember, then a drop toward the warm old endmember (see dashed line in Figure 9c). The oldest two samples from Thiagarajan et al. (2014), dark orange circles that are coeval with our youngest sample, lie near the cold young endmember. The subsequent five samples comprise a depth transect with one shallow and four deep samples (including two top-bottom deep pairs). This depth transect has a temperature inversion—the deep samples are warmer than the shallow sample, and the deep samples record a shift in the radiocarbon value of the water they are growing in toward older values (bottom-to-top shifts are indicated with solid arrows in Figure 9).

The notion that intermediate waters in the North Atlantic were warm during Heinrich Stadial 1 is not new (Dokken et al., 2013; Liu et al., 2009; Marcott et al., 2011), but to reconcile these two deep-sea coral records derived from the same location, we need to imagine a slightly more complicated sequence of events (Figure 9d). At the very beginning of HS1, there is a relatively young, warm water mass in the North Atlantic (Figure 9d, panel 1). This endmember resembles modern AAIW in the equatorial Atlantic, so it could have originated in the south and potentially gained heat via downward diffusion across the thermocline. Between 17.6 and 17.4 ka, there was a shift to cold temperatures at our site. At 17.4 ka, there is a gradual warming and aging trend that continues until 16 ka. This is indicative of water stagnation in the absence of NADW formation (Marcott et al., 2011; Figure 9d, panel 2). These warm waters could then have migrated northward and subducted beneath a halocline, as was proposed by Dokken et al. (2013), and impinged on the base of ice shelves in the North Atlantic, causing them to collapse and triggering the massive discharge of icebergs that marks the Heinrich Event (Figure 9d, panel 3; Bassis et al., 2017; Marcott et al., 2011). As a result of this iceberg discharge, atmospheric circulation adjusts, and we observe the peak Weak Monsoon Interval at ~16.1 ka (see Figure 1f; Wang et al., 2001). During this same time, we see a broad trend toward warmer temperatures in the Southern Ocean, with some variability (Figure 4c). Since the temperature inversion observed by Thiagarajan et al. (2014) near the end of Heinrich Stadial 1 cannot have been caused by local downward diffusion of heat from the surface, observed warm and radiocarbon-depleted intermediate water could have instead come to the North Atlantic from the Southern Ocean perhaps with some additional heat gain at low latitudes, triggering the thermobaric convection that was proposed by Thiagarajan et al. (2014) (Figure 9d, panels 4 and 5). Between 16 ka and the end of HS1, we see a lot variability between the three different endmembers over a relatively short period of time (Figures 9a–9c). This "flickering" between water masses indicates that all of these endmembers are present in the vicinity of our sample site, and different corals record them at different times.

5. Conclusion

We have taken advantage of the unique ability of deep-sea corals to make paired radiocarbon and clumped isotope temperature measurements across the late glacial and deglaciation from the New England and Corner Rise Seamounts in the Northwest Atlantic and from south of Tasmania in the Indo-Pacific sector of the Southern Ocean. Deep-sea corals are able to be independently U/Th-dated and are unaffected by

bioturbation leading to high-resolution reconstructions of past ocean conditions. We find that intermediate waters are highly dynamic throughout the late glacial and deglaciation, indicating that the ocean is not at steady state throughout most of this time, with the possible exception of the LGM. Despite the large amount of variability we observe, we are able to visualize the different ocean endmembers that are present during different times across the deglaciation by making ϵ^{14}C versus temperature crossplots. These crossplots help to give clues as to the mechanisms driving ocean circulation changes at different times.

Deep-sea coral populations wax and wane with local environmental conditions and are probably most sensitive to carbonate ion and oxygen concentrations. In the Southern Ocean, these population dynamics are in sync with measured changes in δ^{13}C across the last 30 kyr, a novel but maybe expected observation given that light ^{13}C values correlate with low carbonate ion and oxygen concentrations. Deep-sea corals grow at the interface between deep δ^{13}C-depleted water and shallow δ^{13}C-enriched water, and the variability that we see in the deep-sea coral data can potentially be attributed to this strong tracer gradient.

Reconstructed temperature and ϵ^{14}C data fall well outside the range of modern data in the adjacent regions of the North Atlantic and Southern Ocean. The prevalence of warm temperatures at intermediate depth during much of the deglaciation supports the hypothesis that the ocean was predominantly salinity stratified rather than temperature stratified. Reconstructed Southern Ocean intermediate water radiocarbon data fall to both sides of the modern value but are largely skewed to younger radiocarbon values. In the Indo-Pacific sector of the Southern Ocean, the main source of old deep water is PDW, so these young radiocarbon values could potentially be explained by a reduction in the influence of PDW at our sample location during the late glacial period and deglaciation. On the other hand, reconstructed North Atlantic intermediate water radiocarbon data are either approximately the same age as the modern ocean or much older. Newly formed NADW is the primary source of young radiocarbon to the Northwest Atlantic, so old radiocarbon values and variability in radiocarbon are indicative of changes in NADW formation. Warm temperatures are observed in the Southern Ocean at the LGM following the peak in Southern Hemisphere summer insolation, indicating local temperature control. In the North Atlantic, warm temperatures are observed during HS1, and they can be attributed to some combination of downward diffusion across the main thermocline during times of NADW reduction and warm water flowing north at intermediate depths from the Southern Ocean.

Acknowledgments
We would like to thank Andrew Thompson, Nivedita Thiagarajan, and Julia Gottschalk for helpful discussions. We also acknowledge constructive comments from two anonymous reviewers. S. K. V. H. received support from NSF Grants OCE-1503129 and OCE-1204211 and the Lamont-Doherty Earth Observatory Postdoctoral Fellowship. All data are available in the supplemental tables and will be archived on the NOAA National Centers for Environmental Information.

References

Adkins, J. F. (2002). The salinity, temperature, and δ^{18}O of the Glacial Deep Ocean. *Science*, *298*(5599), 1769–1773.

Adkins, J. F., Boyle, E. A., Curry, W. B., & Lutringer, A. (2003). Stable isotopes in deep-sea corals and a new mechanism for "vital effects". *Geochimica et Cosmochimica Acta*, *67*(6), 1129–1143.

Adkins, J. F., Cheng, H., Boyle, E. A., Druffel, E. R. M., & Edwards, R. L. (1998). Deep-sea coral evidence for rapid change in ventilation of the Deep North Atlantic 15,400 Years Ago. *Science*, *280*, 725–728.

Adkins, J. F., Griffin, S., Kashgarian, M., Cheng, H., Druffel, E. R. M., Boyle, E. A., et al. (2002). Radiocarbon dating of deep-sea corals. *Radiocarbon*, *44*, 567–580.

Adkins, J. F., Henderson, G. M., Wang, S. L., O'Shea, S., & Mokadem, F. (2004). Growth rates of the deep-sea scleractinia Desmophyllum cristagalli and Enallopsammia rostrata. *Earth and Planetary Science Letters*, *227*(3-4), 481–490.

Adkins, J. F., Ingersoll, A. P., & Pasquero, C. (2005). Rapid climate change and conditional instability of the glacial deep ocean from the thermobaric effect and geothermal heating. *Quaternary Science Reviews*, *24*, 581–594.

Andersen, K. K., Azuma, N., Barnola, J. M., Bigler, M., Biscaye, P., Caillon, N., et al. (2004). High-resolution record of Northern Hemisphere climate extending into the last interglacial period. *Nature*, *431*(7005), 147–151.

Bard, E. (2000). Hydrological impact of Heinrich events in the subtropical northeast Atlantic. *Science*, *289*(5483), 1321–1324.

Barker, S., Diz, P., Vautravers, M. J., Pike, J., Knorr, G., Hall, I. R., & Broecker, W. S. (2009). Interhemispheric Atlantic seesaw response during the last deglaciation. *Nature*, *457*(7233), 1097–1102.

Barnola, J. M., Raynaud, D., Korotkevich, Y. S., & Lorius, C. (1987). Vostok ice core provides 160,000-year record of atmospheric CO_2. *Nature*, *329*, 408–414.

Bassis, J. N., Petersen, S. V., & Mac Cathles, L. (2017). Heinrich events triggered by ocean forcing and modulated by isostatic adjustment. *Nature*, *542*(7641), 332–334.

Bernasconi, S. M., Müller, I. A., Bergmann, K. D., Breitenbach, S. F. M., Fernandez, A., Hodell, D. A., et al. (2018). Reducing uncertainties in carbonate clumped isotope analysis through consistent carbonate-based standardization. *Geochemistry, Geophysics, Geosystems*, *19*, 2895–2914. https://doi.org/10.1029/2017GC007385

Blunier, T., & Brook, E. J. (2001). Timing of millennial-scale climate change in Antarctica and Greenland during the Last Glacial Period. *Science*, *291*(5501), 109–112.

Broecker, W. S. (1998). Paleocean circulation during the last deglaciation: A bipolar seesaw? *Paleoceanography*, *13*, 119–121.

Bryden, H. L., Mujahid, A., Cunningham, S. A., & K. T. (2009). Adjustment of the basin-scale circulation at 26° N to variations in the Gulf Stream, deep western boundary current and Ekman transports as observed by the Rapid array. *Ocean Science*, *5*, 421–433.

Buizert, C., Cuffey, K. M., Severinghaus, J. P., Baggenstos, D., Fudge, T. J., Steig, E. J., et al. (2015). The WAIS divide deep ice core WD2014 chronology—Part 1: Methane synchronization (68–31 ka BP) and the gas age–ice age difference. *Climate of the Past*, *11*(2), 153–173.

Burke, A., & Robinson, L. F. (2012). The Southern Ocean's role in carbon exchange during the Last Deglaciation. *Science*, *335*(6068), 557–561.

Burke, A., Robinson, L. F., McNichol, A. P., Jenkins, W. J., Scanlon, K. M., & Gerlach, D. S. (2010). Reconnaissance dating: A new radiocarbon method applied to assessing the temporal distribution of Southern Ocean deep-sea corals. *Deep-Sea Research Part I-Oceanographic Research Papers*, *57*(11), 1510–1520.

Bush, S. L., Santos, G. M., Xu, X., Southon, J. R., Thiagarajan, N., Hines, S. K., & Adkins, J. F. (2013). Simple, rapid, and cost effective: a screening method for ^{14}C analysis of small carbonate samples. *Radiocarbon*, *55*(3-4), 631–640.

Chappell, J., & Shackleton, N. J. (1986). Oxygen isotopes and sea level. *Nature*, *324*, 137–140.

Chen, S., Gagnon, A. C., & Adkins, J. F. (2018). Carbonic anhydrase, coral calcification and a new model of stable isotope vital effects. *Geochimica et Cosmochimica Acta*, *236*, 179–197.

Chen, T., Robinson, L. F., Burke, A., Southon, J., Spooner, P., Morris, P. J., & Ng, H. C. (2015). Synchronous centennial abrupt events in the ocean and atmosphere during the last deglaciation. *Science*, *349*(6255), 1537–1541.

Cheng, H., Adkins, J. F., Edwards, R. L., & Boyle, E. A. (2000). U-Th dating of deep-sea corals. *Geochimica et Cosmochimica Acta*, *64*, 2401–2416.

Cronin, T. M., Dwyer, G. S., Farmer, J., & Bauch, H. A. (2012). Deep Arctic Ocean warming during the last glacial cycle. *Nature*, *5*, 631–634.

Crowley, T. J. (1992). North Atlantic deep water cools the Southern Hemisphere. *Paleoceanography*, *7*, 489–497.

Curry, W. B., & Oppo, D. W. (2005). Glacial water mass geometry and the distribution of $\delta^{13}C$ of ΣCO_2 in the western Atlantic Ocean. *Paleoceanography*, *20*, PA1017. https://doi.org/10.1029/2004PA001021

De Pol-Holz, R., Keigwin, L., Southon, J., Hebbeln, D., & Mohtadi, M. (2010). No signature of abyssal carbon in intermediate waters off Chile during deglaciation. *Nature Geoscience*, *3*(3), 192–195.

Defliese, W. F., Hren, M. T., & Lohmann, K. C. (2015). Compositional and temperature effects of phosphoric acid fractionation on $\Delta 47$ analysis and implications for discrepant calibrations. *Chemical Geology*, *396*(C), 51–60.

Dennis, K. J., Affek, H. P., Passey, B. H., Schrag, D. P., & Eiler, J. M. (2011). Defining an absolute reference frame for 'clumped' isotope studies of CO_2. *Geochimica et Cosmochimica Acta*, *75*(22), 7117–7131.

Dokken, T. M., Nisancioglu, K. H., Li, C., Battisti, D. S., & Kissel, C. (2013). Dansgaard-Oeschger cycles: Interactions between ocean and sea ice intrinsic to the Nordic seas. *Paleoceanography*, *28*, 491–502. https://doi.org/10.1002/palo.20042

Eiler, J. M. (2007). "Clumped-isotope" geochemistry—The study of naturally-occurring, multiply-substituted isotopologues. *Earth and Planetary Science Letters*, *262*(3-4), 309–327.

Elderfield, H., Yu, J., Anand, P., Kiefer, T., & Nyland, B. (2006). Calibrations for benthic foraminiferal Mg/Ca paleothermometry and the carbonate ion hypothesis. *Earth and Planetary Science Letters*, *250*(3-4), 633–649.

Eltgroth, S. F., Adkins, J. F., Robinson, L. F., Southon, J., & Kashgarian, M. (2006). A deep-sea coral record of North Atlantic radiocarbon through the Younger Dryas: Evidence for intermediate water/deepwater reorganization. *Paleoceanography*, *21*, PA4207. https://doi.org/10.1029/2005PA001192

Emiliani, C. (1955). Pleistocene Temperatures. *The Journal of Geology*, *63*(6), 538–578.

Fernandez, A., Müller, I. A., Rodríguez-Sanz, L., van Dijk, J., Looser, N., & Bernasconi, S. M. (2017). A reassessment of the precision of carbonate clumped isotope measurements: Implications for calibrations and paleoclimate reconstructions. *Geochemistry, Geophysics, Geosystems*, *18*, 4375–4386. https://doi.org/10.1002/2017GC007106

Ferrari, R., Jansen, M. F., Adkins, J. F., Burke, A., Stewart, A. L., & Thompson, A. F. (2014). Antarctic sea ice control on ocean circulation in present and glacial climates. *PNAS*, *111*(24), 8753–8758.

Gagnon, A. C., Adkins, J. F., Fernandez, D. P., & Robinson, L. F. (2007). Sr/Ca and Mg/Ca vital effects correlated with skeletal architecture in a scleractinian deep-sea coral and the role of Rayleigh fractionation. *Earth and Planetary Science Letters*, *261*(1-2), 280–295.

Ghosh, P., Adkins, J. F., Affek, H. P., Balta, B., Guo, W., Schauble, E. A., et al. (2006). ^{13}C–^{18}O bonds in carbonate minerals: A new kind of paleothermometer. *Geochimica et Cosmochimica Acta*, *70*(6), 1439–1456.

Hain, M. P., Sigman, D. M., & Haug, G. H. (2014). Distinct roles of the Southern Ocean and North Atlantic in the deglacial atmospheric radiocarbon decline. *Earth and Planetary Science Letters*, *394*(C), 198–208.

Hemming, S. R. (2004). Heinrich events: Massive late Pleistocene detritus layers of the North Atlantic and their global climate imprint. *Reviews of Geophysics*, *42*, RG1005. https://doi.org/10.1029/2003RG000128

Hines, S. K. V., Southon, J. R., & Adkins, J. F. (2015). A high-resolution record of Southern Ocean intermediate water radiocarbon over the past 30,000 years. *Earth and Planetary Science Letters*, *432*, 46–58.

Huntington, K. W., Eiler, J. M., Affek, H. P., Guo, W., Bonifacie, M., Yeung, L. Y., et al. (2009). Methods and limitations of 'clumped' CO2 isotope (Δ 47) analysis by gas-source isotope ratio mass spectrometry. *Journal of Mass Spectrometry*, *44*(9), 1318–1329.

Huybers, P. J., & Eisenman, I. (2006). Integrated summer insolation calculations. NOAA/NCDC Paleoclimatology Program Data.

Indermühle, A., Monnin, E., Stauffer, B., Stocker, T. F., & Wahlen, M. (2000). Atmospheric CO_2 concentration from 60 to 20 kyr BP from the Taylor Dome Ice Core, Antarctica. *Geophysical Research Letters*, *27*(5), 735–738.

Kelson, J. R., Huntington, K. W., Schauer, A. J., Saenger, C., & Lechler, A. R. (2017). Toward a universal carbonate clumped isotope calibration: Diverse synthesis and preparatory methods suggest a single temperature relationship. *Geochimica et Cosmochimica Acta*, *197*, 104–131.

Key, R., Kozyr, A., Sabine, C., Lee, K., Wanninkhof, R., Bullister, J. L., et al. (2004). A global ocean carbon climatology: Results from Global Data Analysis Project (GLODAP). *Global Biogeochemical Cycles*, *18*, GB4031. https://doi.org/10.1029/2004GB002247

Lamy, F., Kaiser, J., Arz, H. W., Hebbeln, D., Ninnemann, U., Timm, O., et al. (2007). Modulation of the bipolar seesaw in the Southeast Pacific during Termination 1. *Earth and Planetary Science Letters*, *259*(3-4), 400–413.

Lemieux-Dudon, B., Blayo, E., Petit, J.-R., Waelbroeck, C., Svensson, A., Ritz, C., et al. (2010). Consistent dating for Antarctic and Greenland ice cores. *Quaternary Science Reviews*, *29*(1-2), 8–20.

Lippold, J., Grützner, J., Winter, D., Lahaye, Y., Mangini, A., & Christl, M. (2009). Does sedimentary $^{231}Pa/^{230}Th$ from the Bermuda Rise monitor past Atlantic meridional overturning circulation? *Geophysical Research Letters*, *36*, L12601. https://doi.org/10.1029/2009GL038068

Liu, Z., Otto Bliesner, B. L., He, F., Brady, E. C., Tomas, R., Clark, P. U., et al. (2009). Transient simulation of last deglaciation with a new mechanism for Bolling-Allerod warming. *Science*, *325*(5938), 310–314.

Lomitschka, M., & Mangini, A. (1999). Precise Th/U-dating of small and heavily coated samples of deep sea corals. *Earth and Planetary Science Letters*, *170*(4), 391–401.

Lund, D. C., Adkins, J. F., & Ferrari, R. (2011). Abyssal Atlantic circulation during the Last Glacial Maximum: Constraining the ratio between transport and vertical mixing. *Paleoceanography*, *26*, PA1213. https://doi.org/10.1029/2010PA001938

Marcott, S. A., Bauska, T. K., Buizert, C., Steig, E. J., Rosen, J. L., Cuffey, K. M., et al. (2014). Centennial-scale changes in the global carbon cycle during the last deglaciation. *Nature*, *514*, 616–619.

Marcott, S. A., Clark, P. U., Padman, L., Klinkhammer, G. P., Springer, S. R., Liu, Z., et al. (2011). Ice-shelf collapse from subsurface warming as a trigger for Heinrich events. *PNAS*, *108*(33), 13,415–13,419.
Martin, P. A., Lea, D. W., Rosenthal, Y., & Shackleton, N. J. (2002). Quaternary deep sea temperature histories derived from benthic foraminiferal Mg/Ca. *Earth and Planetary Science Letters*, *198*(1-2), 193–209.
McManus, J. F., Francois, R., Gherardi, J. M., Keigwin, L. D., & Brown-Leger, S. (2004). Collapse and rapid resumption of Atlantic meridional circulation linked to deglacial climate changes. *Nature*, *428*(6985), 834–837.
Mitsuguchi, T., Matsumoto, E., Abe-Ouchi, A., Uchida, T., & Isdale, P. J. (1996). Mg/Ca thermometry in coral skeletons. *Science*, *274*, 961–963.
Monnin, E., Indermühle, A., Dällenbach, A., Flückiger, J., Stauffer, B., Stocker, T. F., et al. (2001). Atmospheric CO2 concentrations over the last glacial termination. *Science*, *291*(5501), 112–114.
Nurnberg, D., Bijma, J., & Hemleben, C. (1996). Assessing the reliability of magnesium in foraminiferal calcite as a proxy for water mass temperatures. *Geochimica et Cosmochimica Acta*, *60*(5), 803–814.
Orsi, A. H., Whitworth, T. III, & Nowlin, JrW. D. (1995). On the meridional extent and fronts of the Antarctic Circumpolar Current. *Deep-Sea Research Part I-Oceanographic Research Papers*, *42*(5), 641–673.
Passey, B. H., Levin, N. E., Cerling, T. E., Brown, F. H., & Eiler, J. M. (2010). High-temperature environments of human evolution in East Africa based on bond ordering in paleosol carbonates. *Proceedings of the National Academy of Sciences*, *107*(25), 11,245–11,249.
Petit, J. R., Jouzel, J., Raynaud, D., Barkov, N. I., Barnoula, J.-M., Basile, I., et al. (1999). Climate and atmospheric history of the past 420,000 years from the Vostok ice core, Antarctica. *Nature*, *399*, 429–436.
Rasmussen, S. O., Bigler, M., Blockley, S. P., Blunier, T., Buchardt, S. L., Clausen, H. B., et al. (2014). A stratigraphic framework for abrupt climatic changes during the Last Glacial period based on three synchronized Greenland ice-core records: Refining and extending the INTIMATE event stratigraphy. *Quaternary Science Reviews*, *106*, 14–28.
Reimer, P. J., Baillie, M. G. L., Bard, E., Bayliss, A., Beck, J. W., Blackwell, P. G., et al. (2009). IntCal09 and Marine09 radiocarbon age calibration curves, 0–50,000 years cal BP. *Radiocarbon*, *51*, 1111–1150.
Reimer, P. J., Bard, E., Bayliss, A., Beck, J. W., Blackwell, P. G., Ramsey, C. B., et al. (2013). IntCal13 and Marine13 radiocarbon age calibration curves 0–50,000 years cal BP. *Radiocarbon*, *55*(4), 1869–1887.
Robinson, L. F., Adkins, J. F., Keigwin, L. D., Southon, J., Fernandez, D. P., Wang, S. L., & Scheirer, D. S. (2005). Radiocarbon variability in the Western North Atlantic during the last deglaciation. *Science*, *310*, 1469–1473.
Rosenthal, Y., Boyle, E. A., & Slowey, N. (1997). Temperature control on the incorporation of magnesium, strontium, fluorine, and cadmium into benthic foraminiferal shells from Little Bahama Bank: Prospects for thermocline paleoceanography. *Geochimica et Cosmochimica Acta*, *61*(17), 3633–3643.
Saenger, C., Affek, H. P., Felis, T., Thiagarajan, N., Lough, J. M., & Holcomb, M. (2012). Carbonate clumped isotope variability in shallow water corals: Temperature dependence and growth-related vital effects. *Geochimica et Cosmochimica Acta*, *99*(C), 224–242.
Shackleton, N. J. (1967). Oxygen isotope analyses and Pleistocene temperature re-assessed. *Nature*, *215*, 1–3.
Sigman, D. M., & Boyle, E. A. (2000). Glacial/interglacial variations in atmospheric carbon dioxide. *Nature*, *407*, 859–869.
Sikes, E. L., Elmore, A. C., Allen, K. A., Cook, M. S., & Guilderson, T. P. (2016). Glacial water mass structure and rapid $\delta^{18}O$ and $\delta^{13}C$ changes during the last glacial termination in the Southwest Pacific. *Earth and Planetary Science Letters*, *456*, 87–97.
Skinner, L. C., Fallon, S., Waelbroeck, C., Michel, E., & Barker, S. (2010). Ventilation of the deep Southern Ocean and deglacial CO_2 rise. *Science*, *328*(5982), 1147–1151.
Skinner, L., McCave, I. N., Carter, L., Fallon, S., Scrivner, A. E., & Primeau, F. (2015). Reduced ventilation and enhanced magnitude of the deep Pacific carbon pool during the last glacial period. *Earth and Planetary Science Letters*, *411*(C), 45–52.
Soulet, G., Skinner, L. C., Beaupré, S. R., & Galy, V. (2016). A note on reporting of reservoir ^{14}C disequilibria and age offsets. *Radiocarbon*, *58*(1), 205–211.
Spooner, P. T., Guo, W., Robinson, L. F., Thiagarajan, N., Hendry, K. R., Rosenheim, B. E., & Leng, M. J. (2016). Clumped isotope composition of cold-water corals: A role for vital effects? *Geochimica et Cosmochimica Acta*, *179*(C), 123–141.
Stuiver, M., & Polach, H. A. (1977). Reporting of C-14 Data - Discussion. *Radiocarbon*, *19*(3), 355–363.
Stuiver, M., Quay, P. D., & Ostlund, H. G. (1983). Abyssal water carbon-14 distribution and the age of the World Oceans. *Science*, *219*(4586), 849–851.
Su, Z., He, F., & Ingersoll, A. P. (2016). On the abruptness of Bølling–Allerød warming. *Journal of Climate*, *29*(13), 4965–4975.
Talley, L. (2013). Closure of the global overturning circulation through the Indian, Pacific, and Southern Oceans: Schematics and transports. *Oceanography*, *26*(1), 80–97.
Thiagarajan, N., Adkins, J. F., & Eiler, J. M. (2011). Carbonate clumped isotope thermometry of deep-sea corals and implications for vital effects. *Geochimica et Cosmochimica Acta*, *75*(16), 4416–4425.
Thiagarajan, N., Gerlach, D., Roberts, M. L., Burke, A., McNichol, A. P., Jenkins, W. J., et al. (2013). Movement of deep-sea coral populations on climatic timescales. *Paleoceanography*, *28*, 227–236. https://doi.org/10.1002/palo.20023
Thiagarajan, N., Subhas, A. V., Southon, J. R., Eiler, J. M., & Adkins, J. F. (2014). Abrupt pre-Bølling-Allerød warming and circulation changes in the deep ocean. *Nature*, *511*, 75–78.
Thornalley, D. J. R., Bauch, H. A., Gebbie, G., Guo, W., Ziegler, M., Bernasconi, S. M., et al. (2015). A warm and poorly ventilated deep Arctic Mediterranean during the last glacial period. *Science*, *349*(6249), 706–710.
WAIS Divide Project Members (2013). Onset of deglacial warming in West Antarctica driven by local orbital forcing. *Nature*, *500*(7463), 440–444.
Wang, Y. J., Cheng, H., Edwards, R. L., An, Z., Wu, J. Y., Shen, C.-C., & Dorale, J. A. (2001). A high-resolution absolute-dated Late Pleistocene monsoon record from Hulu Cave, China. *Science*, *294*(5550), 2345–2348.
Wang, Z., & Schauble, E. (2004). Equilibrium thermodynamics of multiply substituted isotopologues of molecular gases. *Geochimica et Cosmochimica Acta*, *68*, 4779–4797.